THE JOURNAL OF PHYSICAL CHEMISTRY B

Article

pubs.acs.org/JPCB

Diffusive Nature of Xenon Anesthetic Changes Properties of a Lipid Bilayer: Molecular Dynamics Simulations

Eiji Yamamoto,[†] Takuma Akimoto,[†] Hiroyuki Shimizu,[†] Yoshinori Hirano,[‡,§] Masato Yasui,[§] and Kenji Yasuoka[†,*]

[†]Department of Mechanical Engineering, Keio University, 3-4-1 Hiyoshi, Kohoku-ku, Yokohama 223-8522, Japan

[‡]Laboratory for Computational Molecular Design, Computational Biology Research Core, Quantitative Biology Center (QBiC), The Institute of Physical and Chemical Research (RIKEN), 1-6-5 minatojima-minami machi, Chuo-ku, Kobe, Hyogo 650-0047, Japan

[§]Department of Pharmacology, Keio University School of Medicine, 35 Shinanomachi, Shinju-ku, Tokyo 160-8582, Japan

Supporting Information

ABSTRACT: Effects of general anesthesia can be controllable by the ambient pressure. We perform molecular dynamics simulations for a 1-palmitoyl-2-oleoyl phosphatidylethanolamine lipid bilayer with or without xenon molecules by changing the pressure to elucidate the mechanism of the pressure reversal of general anesthesia. According to the diffusive nature of xenon molecules in the lipid bilayer, a decrease in the orientational order of the lipid tails, an increase in the area and volume per lipid molecule, and an increase in the diffusivity of lipid molecules are observed. We show that the properties of the lipid bilayer with xenon molecules at high pressure come close to those without xenon molecules at 0.1 MPa. Furthermore, we find that xenon molecules are concentrated in the middle of the lipid bilayer at high pressures by the pushing effect and that the diffusivity of xenon molecules is suppressed. These results suggest that the pressure reversal originates from a jamming and suppression of the diffusivity of xenon molecules in lipid bilayers.

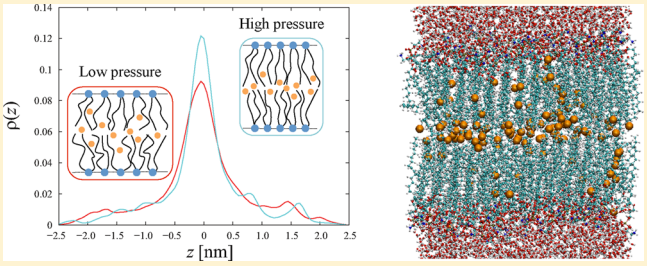

INTRODUCTION

General anesthesia has been widely used in surgical operations. However the mechanism of how it works has not been fully elucidated. There is no common structure in general anesthetics. It thus seems that the mechanism is related to not only static but also dynamical characteristics of general anesthetics in membranes. The pressure reversal of general anesthesia is a clue to elucidate its mechanism. The swimming motion of tadpoles disappears when they are anesthetized with an ethanol liquid, which reappears when the anesthetized tadpoles are exposed to a hydrostatic pressure of 13−35 MPa.[1] The pressure reversal of anesthesia is also confirmed for tadpoles by using many kinds of clinical and unconventional anesthetics.[2] Furthermore, the pressure reversal of general anesthesia for newts and mice has also been demonstrated experimentally.[3−5]

There are two hypotheses for the mechanism of general anesthesia: the membrane hypothesis and the protein receptor hypothesis.[6] The object of the former is membrane lipids, while the latter is membrane proteins.

The membrane hypothesis is supported by the Meyer−Overton law.[7,8] This is a rule of thumb in the relation between solubility in oil and action strength of anesthesia. An anesthetic that dissolves readily in olive oil demonstrates a strong effect of anesthesia. Recently, Heimburg and Jackson proposed a thermodynamic extension of the Meyer−Overton law based on free energy changes.[9] An increase in the amount of methoxyflurane or halothane in a membrane generates an increase of the orientational order,[10] and this change of the orientational order is reversed at 27.4 MPa.[11] The effects of general anesthetics on membranes have been studied by molecular dynamics (MD) simulations at atmospheric[12−18] and high pressures.[19−21] Cantor proposed that general anesthetics perturb the pressure profile in a membrane and cause conformation changes of proteins.[22,23] The MD simulations of a dimyristoylphosphatidylcholine (DMPC) bilayer with 1-alkanols at 0.1 MPa revealed that 1-alkanols change the pressure profiles of the lipid bilayer. However, the change of the pressure profiles are not reversed at 100 MPa.[19] Chau et al. showed that halothane molecules embedded in a DMPC membrane tend to cluster together at high pressures (20, 40 MPa)[20,21] and proposed that the pressure reversal occurs when halothane molecules aggregate and cannot bind to the putative binding site because the cluster size is too big to reach the binding site for haloalkane general anesthesia in the $GABA_A$ receptor.[24]

Recent experiments regarding the protein receptor hypothesis have shown that ion channels, *N*-methyl-D-aspartic acid

Received: April 7, 2012
Revised: May 23, 2012
Published: June 20, 2012

   dx.doi.org/10.1021/jp303330c | *J. Phys. Chem. B* 2012, 116, 8989−8995

receptor (NMDA receptor) and $GABA_A$ receptor et al., are molecular targets for general anesthesia.[6,25] Xenon is a general anesthetic which has pharmacological benefits,[26−33] and inhibits the NMDA receptor.[34−36] Mutations (F639A in NR1 and A825w in NR2A) of the NMDA receptor reduce the anesthetic sensitivity.[37] Potential xenon action sites in the ligand binding domain of the NMDA receptor is identified by a grand canonical Monte Carlo simulation[38]and MD simulation.[39] However, other research shows that inhibition of the NMDA receptor with xenon requires the AMPA receptor, which is a glutamatergic receptor,[40] whereas nitrous oxide actions do not require the AMPA receptor in *Caenorhabditis elegans* (*C. elegans*).[41]

There are a large number of studies about the effects of general anesthetics on the altered function of the $GABA_A$ receptor.[34,42−46] For example, mutations in the $GABA_A$ receptor reduce the anesthetic sensitivity. However, most studies have indicated that xenon has minimal effects on the $GABA_A$ function.[34,35,47] Crystal structures of the complexes propofol/GLIC and desflurane/GLIC, a pentameric ligand gated ion channel of the same cys-loop family as $GABA_A$, have been observed.[48] A common binding site for general anesthetics exists within each subunit of the apo-structure in the upper part of the transmembrane domain of each protomer. Xenon and etomidate modulate GLIC at or above clinical concentrations.[49] Ivermectin, which inhibits neurotransmission, binds with glutamate-gated chloride channel (GluCl), and the binding site is within each subunit interfaces in the upper part of the transmembrane domains.[50] The mechanism of general anesthesia remaines unclear.

In this paper, we perform MD simulations of a 1-palmitoyl-2-oleoyl phosphatidylethanolamine (POPE) bilayer with or without xenon molecules at several pressures (0.1, 10, 20, 35, and 50 MPa) to validate the relation between the diffusive nature of anesthetics in the lipid bilayer and properties of the lipid bilayer.

METHOD

To elucidate the mechanism of the pressure reversal of general anesthesia, MD simulations for a POPE bilayer with or without xenon molecules at several pressures were performed. We constructed the initial structure of a lipid bilayer membrane system containing 128 POPE molecules with 10 004 TIP3P water molecules (noXe-POPE) and a system containing 128 POPE molecules with 9876 TIP3P water molecules and 128 xenon molecules (Xe-POPE) (see Figure 1). Xenon molecules were put uniformly into the hydrophobic group of the POPE bilayer. We minimized their energy using the conjugate gradient method after the steepest descent method. A 200 ns simulation of noXe-POPE using a constant number of atoms at a pressure of 0.1 MPa and a temperature of 310 K was performed, and the final structure of the simulation was defined to be the standard structure. We performed an additional four 40 ns simulations at several pressures (10, 20, 35, and 50 MPa) using the standard structure. To observe the dynamics of xenon molecules, we performed 120, 120, 120, 80, and 150 ns simulations for Xe-POPE at 0.1, 10, 20, 35, and 50 MPa, respectively. All MD simulations were carried out using a constant number of atoms, pressure, and temperature of 310 K, where the Berendsen's algorithm with a coupling time of 0.2 ps was used. The time step was set at 1 fs. The bond lengths involving the hydrogen atoms were constrained to equilibrium lengths using the SHAKE method. The GAFF force field was

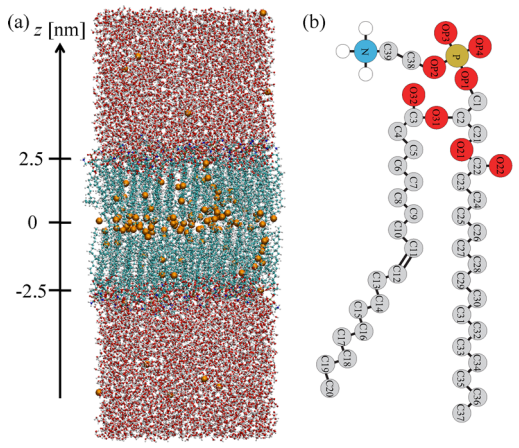

Figure 1. Schematic view of this study. (a) Snapshot of the simulation system with xenon molecules. Lipid bilayer, water molecules, and xenon molecules show green, red, and orange, respectively. (b) Structural formula of POPE [1-palmitoyl-2-oleoyl phosphatidylethanolamine(18:1)] lipid molecule (red, brown, light blue, and gray circles indicate oxygen, phosphorus, nitrogen, and carbon atoms, respectively.).

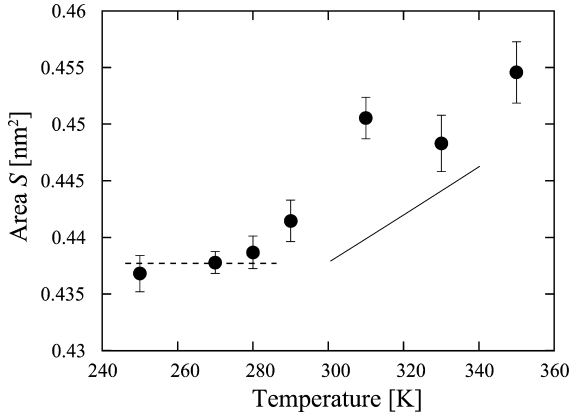

Figure 2. Area per lipid S at different temperatures. Circles with error bars are the result of MD simulations. Areas from 250 to 280 K are almost constant, and areas above 280 K notably increase. This suggests that transition temperature is around 280 K. The dashed line is the average area from 250 to 280 K, and the solid line is the increasing rate of areas from 280 to 350 K calculated by the least-squares method.

used for the POPE lipid. This parameter of POPE has been used in previous studies about the membrane or a membrane protein.[51,52] The Lennard-Jones potential was used for the force field for the xenon molecules.[53] The particle mesh Ewald method was used, and the direct space cutoff distance was set to 1.0 nm. A three-dimensional periodic boundary condition was employed for all systems. We used the trajectories of the last 20 ns to analyze the properties of each system. MD simulations were performed using AMBER10 software.[54]

The lipid bilayer changes from gel to liquid-crystalline phase at a temperature. This temperature is estimated from a relationship between the temperature and area per lipid. It has been confirmed that the transition temperature is estimated at about 280 K in a previous simulation of POPE bilayer.[55] To estimate the transition temperature in our model, additional 60−90 ns simulations were performed at several temperatures (250, 270, 280, 290, 330, 350 K) using the standard structure. As shown in Figure 2, the transition temperature is estimated to

dx.doi.org/10.1021/jp303330c | J. Phys. Chem. B 2012, 116, 8989−8995

be about 280 K; thus, the POPE bilayer at 310 K is liquid-crystalline state. We note that the area per lipid at 310 K is smaller than experimental data[56] and almost the same as other MD simulations,[55,57,58] indicating that the POPE bilayer is a little stiff in our simulations.

RESULTS

Property of xenon molecule. *Density of Xenon Molecules.* The density of the z position of xenon molecules

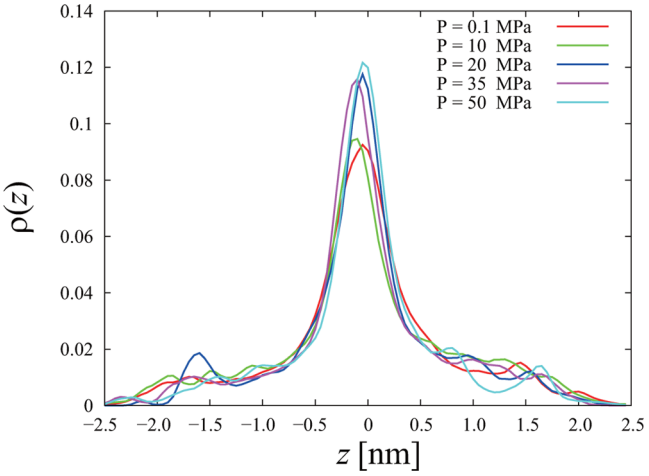

Figure 3. Density of the z position of xenon molecules, where the z axis is normal to the lipid bilayer. The center of the lipid bilayer is z = 0 nm, and the upper and lower surface of the lipid bilayer are around 2.5 and −2.5 nm, respectively. Different color curves are the densities at different pressures. The numbers of xenon molecules in the lipid bilayer at 0.1, 10, 20, 35, and 50 MPa are 114, 113, 106, 112, and 119, respectively.

in the lipid bilayer is determined by the sojourn time of each particle. The probability of the ith particle in $[z,z+dz)$, $\rho^i(z)\,dz$, is given by

$$\rho^i(z)\,dz = \frac{1}{T}\int_0^T 1_{[z,z+dz)}(z^i(t))\,dt \tag{1}$$

At long times ($T \to \infty$), $\rho^i(z)$ does not depend on the particle number i, and is equal to the ensemble average if ergodicity holds. The time and ensemble averaged density of the z position is taken as

$$\rho(z)\,dz = \frac{1}{N_{Xe}}\sum_{i=1}^{N_{Xe}}\rho^i(z) \tag{2}$$

where N_{Xe} is the number of xenon molecules in the lipid bilayer. The numbers of xenon molecules that remain within the lipid bilayer during simulations at 0.1, 10, 20, 35, and 50 MPa are 114, 113, 106, 112, and 119, respectively. Figure 3 shows the densities of the z direction of xenon molecules at each pressure. The peak of the density of xenon molecules is at the center of the lipid bilayer for all pressures. We note that xenon molecules are jammed at the center of the lipid bilayer when the pressure is increased. Some xenon molecules are trapped for a long time away from the center of the lipid bilayer, and thus the densities slightly fluctuate. In particular, the peak of the density at $z \cong -1.7$ nm for P = 20 MPa is a result of trappings. We have confirmed the density of xenon molecules at 350 K under 0.1 and 50 MPa to clarify whether xenon molecules really do not go outside from the lipid bilayer

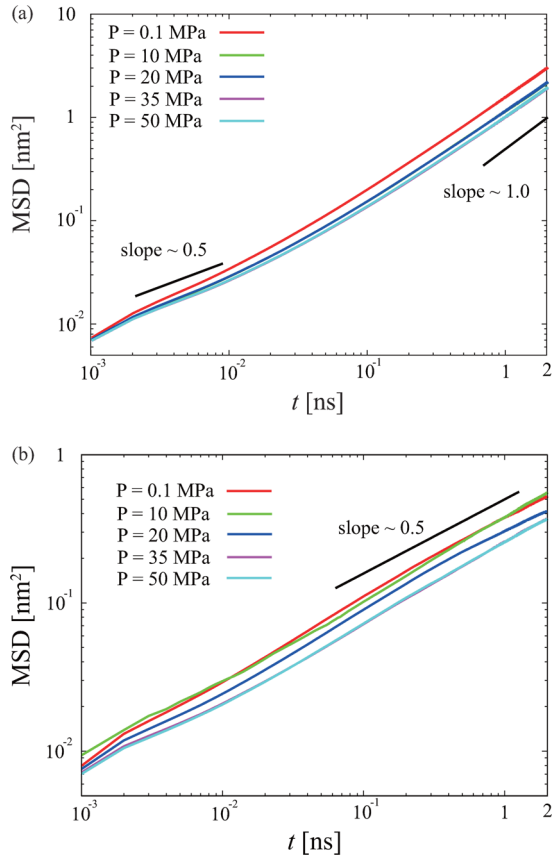

Figure 4. (a) Lateral MSD of xenon molecules (T = 20 ns). (b) MSD of xenon molecules for the z direction (T = 20 ns). MSDs are calculated by using xenon molecules inside the lipid bilayer. Different color curves are the MSD at different pressures. For reference, the scaling exponents of the MSD, α, are represented by the solid lines.

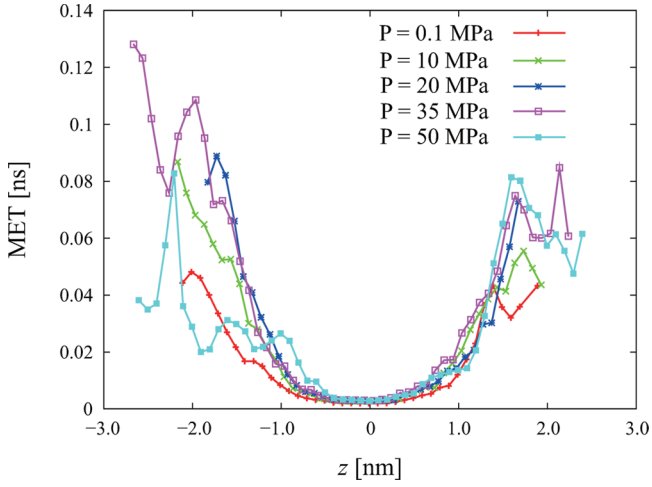

Figure 5. Mean exit time for xenon molecules at different pressures. Exit times are obtained by different xenon molecules inside the lipid bilayer. The horizontal axis, z, is the same as in Figure 3.

at the high pressure. In spite of the high temperature, xenon molecules exist in the lipid bilayer and the peak of the density is at the center of the lipid bilayer (Figure S1 of the Supporting Information).

Diffusion of Xenon Molecules. The time averaged mean square displacement (TAMSD) for each particle is defined by

dx.doi.org/10.1021/jp303330c | J. Phys. Chem. B 2012, 116, 8989−8995

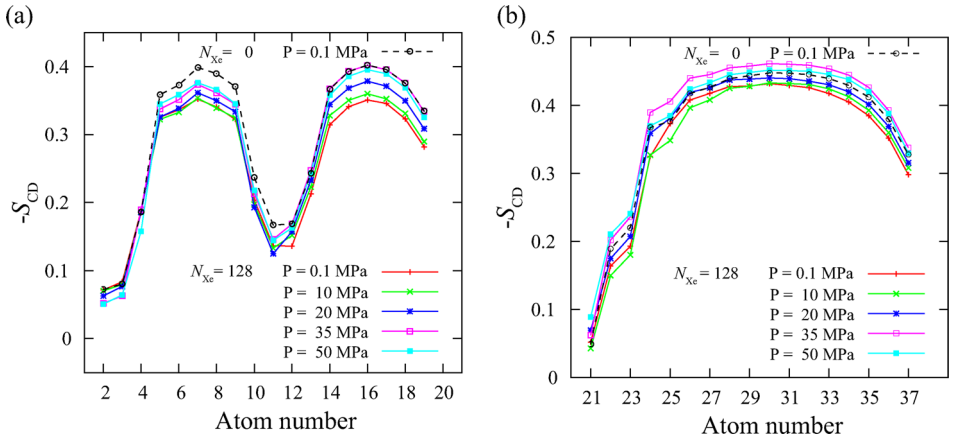

Figure 6. Orientational order parameter SCD of lipid tails for (a) C2−C20 and (b) C2, C21−C37. The atom number, *i*, is labeled with reference to C2 in Figure 1b, namely, *i* = 1−20 for C2, O31, C3, C4−C20, and *i* = 21−38 for C21, O21, C22, C23−C37. Color curves are the results of the systems with xenon molecules at different pressures, and the black dashed curve is the result of the system without xenon molecules at 0.1 MPa.

$$\overline{x^2(t)} \equiv \frac{1}{T-t}\int_0^{T-t} \{x(t'+t) - x(t')\}^2 \, dt' \tag{3}$$

Mean square displacement (MSD) is the average of TAMSD with respect to particles. In Figure 4a, lateral MSD, $\langle\overline{l^2(t)}\rangle \equiv (\langle\overline{x^2(t)}\rangle + \langle\overline{y^2(t)}\rangle)/2$, grows sublinearly for a short time, and after that it increases linearly in time [three-dimensional MSD of xenon molecule, $\langle\overline{r^2(t)}\rangle \equiv (\langle\overline{x^2(t)}\rangle + \langle\overline{y^2(t)}\rangle + \langle\overline{z^2(t)}\rangle)/3$, shows similar behavior of lateral MSD though xenon molecules are confined in the *z* direction by the lipid bilayer]:

$$\langle\overline{l^2(t)}\rangle \propto \begin{cases} t^{\alpha} & (t < t_c) \\ t & (t > t_c) \end{cases} \tag{4}$$

where $\langle - \rangle$ denotes the average with respect to both time and particle, and the subdiffusive exponent α is almost equal to 0.5. This phenomenon is called a transient subdiffusion. Transient subdiffusions are observed at every pressure, and exponent α is about 0.5 except for the case of atmosphere, where the exponent is about 0.8. The crossover time from subdiffusion to normal diffusion is about t_c = 0.001−0.1 ns. Diffusion tends to be suppressed according to the increase of the pressure. Figure 4b shows the MSD of the *z* direction of the xenon molecule. Surprisingly, in spite of the confinement according to the lipid bilayer in the *z* direction, xenon molecules show suddiffusion in the time interval that we analyzed. Moreover, the exponent of the subdiffusion is almost 0.5 for all pressures [this is because the time difference *t* is shorter than the time showing the effect of the confinement; however, the cause of subdiffusion is not clear].

Mean Exit Time. To quantify the diffusivity in the lateral direction, we calculate the mean exit time (MET) restricted to the initial point *z*. In particular, the MET restricted to *z* is the mean of the exit time, defined as

$$T_{MET}(z) \equiv \min\{t | \Delta r(t) > \Delta_c\} \tag{5}$$

where $\Delta r(t) = (\{x(t+t_0) - x(t_0)\}^2 + \{y(t+t_0) - y(t_0)\}^2)^{1/2}$, and $z(t_0) = z$. In this case, Δ_c is 0.01 nm. Although xenon molecules can move to the *z* direction while $\Delta r < \Delta_c$, T_{MET} is a good quantity for characterizing diffusivity. The inverse of MET relates to the diffusion coefficient, namely, diffusivity. In Figure 5, the xenon molecule has a high diffusivity at the center of the lipid bilayer and low diffusivity away from the center of the lipid bilayer.

Property of Lipid Bilayer. In the following, we study the properties of the lipid bilayer, such as the orientational order parameter, volume, area, thickness, and diffusivity at different pressures.

Orientational Order Parameter S_{CD}. The orientational order parameter S_{CD}[59] is an amount that provides how well a molecule lines up for a director, and it is given by

$$-S_{CD} = \frac{2}{3}S_{xx} + \frac{1}{3}S_{yy}$$

$$S_{\alpha\beta} = \frac{1}{2}\langle\overline{3\cos\theta_\alpha \cos\theta_\beta - \delta_{\alpha\beta}}\rangle, \quad \alpha, \beta = x, y, z$$

$$\cos\theta_\alpha = \hat{e}_\alpha \cdot \hat{e}_k \tag{6}$$

where $\hat{e}_k$ is the director vector, $\hat{e}_x$ is a unit vector perpendicular to vector $e_{i,i+2}$, $e_{i,i+2}$ is the unit vector from A_i to A_{i+2} which is contained in the plane formed by the *i*, *i*+1, *i*+2 particles, θ_x is the angle between $\hat{e}_k$ and $\hat{e}_x$, and θ_y is the angle between $\hat{e}_k$ and the unit $\hat{e}_y$ which is perpendicular to the plane formed by the *i*, *i*+1, *i*+2 particles.

Figure 6 shows S_{CD} of C2−C20 and C2, C21−C37. The point of bending in Figure 6a is a double bond (C11−C12) in the lipid tail. This order parameter shows higher value than experimental data[55] and simulation data[60] because of a little stiff model of the lipid bilayer. The value of S_{CD} in the system with xenon molecules (0.1 MPa) is lower than that without xenon molecules (0.1 MPa) because xenon molecules diffuse in the lipid bilayer and collide against the lipid tails.

According to an increase in pressure, the shape of S_{CD} in the system with xenon molecules comes close to that without xenon molecules (0.1 MPa). The value of $-S_{CD}$ becomes higher in all systems according to the increase of the pressure, which means that the direction of the lipid tails is aligned by pressure.

Volume, Area, and Thickness. Figure 7 shows volume per lipid, area per lipid, and the thickness of the lipid bilayer (plane normal to the *z* axis). The thickness of the lipid bilayer *h* is the distance between the average *z* position of the nitrogen atom in the upper membrane $\langle z_{top}(t)\rangle$ and the lower membrane $\langle z_{bottom}(t)\rangle$, given by

$$h = \frac{1}{T}\int_0^T \{\langle z_{top}(t)\rangle - \langle z_{bottom}(t)\rangle\} \, dt \tag{7}$$

dx.doi.org/10.1021/jp303330c | J. Phys. Chem. B 2012, 116, 8989−8995

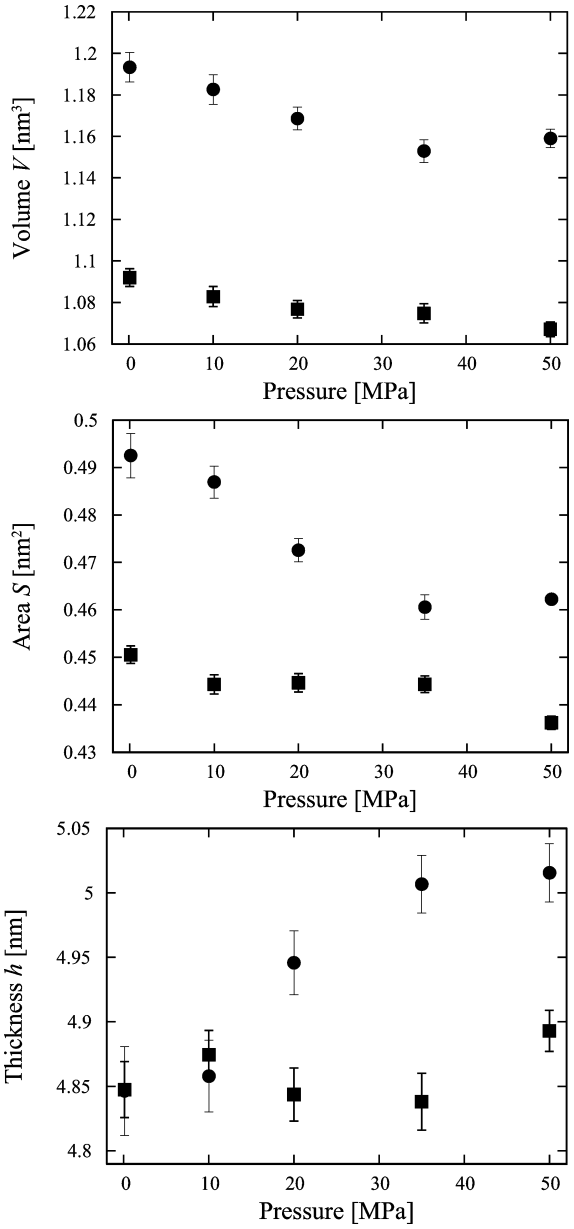

Figure 7. Volume per lipid$V$, area per lipid S, and thickness of the lipid bilayer h at different pressures. Circle and square symbols are the results of the systems with and without xenon molecules, respectively. Error bars mean the root-mean-square deviations.

The area per lipid S is obtained by dividing the x,y plane of the simulation box by the number of lipid molecules. The volume per lipid V is defined as $V = Sh/2$.

Generally, when V becomes low at high pressures, S and h become small. In the system with xenon molecules, V and S increase because the xenon molecules are concentrated in the lipid bilayer. According to an increase in pressure, S in the system with xenon molecules comes close to that without xenon molecules (0.1 MPa). S in the system with xenon molecules decreases greater than that without xenon molecules according to an increase in pressure. This is because there is an additional reduction in the area occupied by xenon molecules in the system with xenon molecules. In the system with xenon molecules, V decreases according to the increase of the pressure but does not come close to that without xenon molecules (0.1 MPa) at a high pressure because h increases according to an increase in pressure. This unexpected increase in h originates from the increase in orientational order parameters of lipid tails and no change of the gap between the terminal carbons of the two bilayer leaflets (see Figure S2 of the Supporting Information). Thickness h is affected by two factors: xenon molecules at the center of the lipid bilayer and the orientational order parameters of lipid tails. In Figure 6, the order parameters decrease by the effects of xenon molecules at atmospheric pressure, and this decreasing reduces the thickness of the hydrophobic region of each leaflet. The localization of xenon molecules at the center of the lipid bilayer increases the gap. At 0.1 and 10 MPa, the decreasing of the order parameters and the localization of xenon molecules cancel the effects on h. When the pressure increases, the gap between the terminal carbons does not change, whereas the thickness of the hydrophobic region of each leaflet increases because of the increase in S_{CD}. Therefore, h increases in the system with xenon molecules according to the increase in pressure.

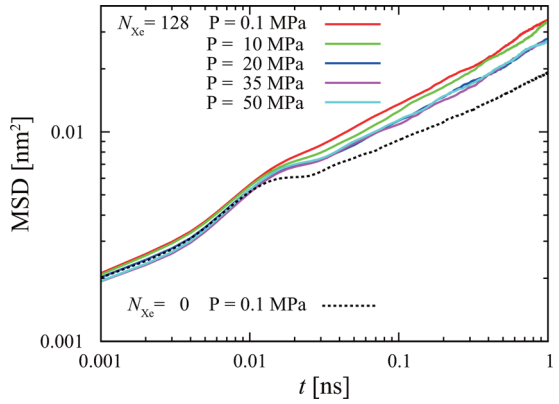

Figure 8. Lateral MSD of lipid molecules (T = 1 ns). Color curves are the results of the systems with xenon molecules at different pressures, and the black dashed curve is the result of the system without xenon molecules at 0.1 MPa.

MSD of Lipid Molecule. In the center-of-mass motion of lipid molecules, there are three different scaling in MSD.[61] In a short time regime, the lipid molecule shows a ballistic motion by the vibration of the lipid molecule. Transient subdiffusion is observed in the following comparatively short time region, and the lipid molecule is trapped by molecular crowding, which generates non-Gaussian fluctuations in TAMSDs.[52] The lateral MSD of the lipid molecule, $\langle\overline{l^2(t)}\rangle$, shows

$$\langle\overline{l^2(t)}\rangle \propto \begin{cases} t^2 \text{ (ballistic)} \\ t^{\alpha} \text{ (subdiffusion)} \\ t \text{ (normal)} \end{cases} \quad (8)$$

In this study, diffusivity of the lipid molecule was evaluated by MSD in the subdiffusive region. Figure 8 shows the MSD of the lipid molecule, where we use trajectories of the C2 atom. This MSD is subtracted by the center of mass of the lipid bilayer.

The MSD in the system with xenon molecules is bigger than that without xenon molecules. The motion of the xenon molecules and increase in the area per lipid enhance the diffusivity of the lipid bilayer. According to an increase in pressure, the MSD in the system with xenon molecules comes close to that without xenon molecules (0.1 MPa). Since the area per lipid becomes small and xenon molecules are

dx.doi.org/10.1021/jp303330c | J. Phys. Chem. B 2012, 116, 8989−8995

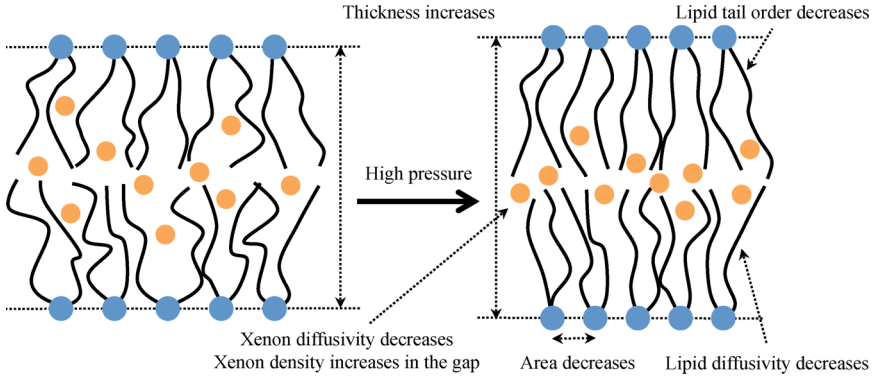

Figure 9. Schematic model depicting the pushing effect of xenon molecules at high pressures. Blue circles are lipid head groups, black lines are lipid tails, and orange circles are xenon molecules.

concentrated in the center of the lipid bilayer at high pressure, the diffusivity of the lipid molecules decreases.

DISCUSSION

By extensive MD simulations, we found that xenon molecules diffuse in the POPE bilayer and change the properties of the POPE bilayer. In the system with xenon molecules, decreasing of orientational order parameter of lipid tails, increasing in area and volume per lipid molecule, and increasing in diffusivity of lipid molecules are observed. These changes are almost the same as those in a DPPC bilayer with xenon molecules except for the orientational order parameter[15] but are different from those in a DMPC bilayer containing 1-alkanol molecules.[17] In the DMPC bilayer with 1-alkanol, decreasing in area, increasing in orientational order of the lipid tails, and suppression of diffusivity of lipids are observed. We found that the POPE bilayer pushes out xenon molecules to the interspace between the upper and lower membrane at high pressures (Figure 9). Xenon molecules are jammed by the pushing effect, and the diffusivity of xenon molecules is suppressed at high pressures. Moreover, properties of the POPE bilayer with xenon molecules at high pressures come close to those without xenon molecules at 0.1 MPa. It is interesting to note that the thickness of the POPE bilayer in the system with xenon molecules increases according to an increase in pressure. Although POPE bilayers in our simulations are a little stiff, this difference will not affect the diffusive nature of xenon molecules. We conclude that the diffusive nature of xenon anesthetics changes properties of membranes.

Koltchine et al. reported that substitutions of Ser270 in the $GABA_A$ decrease potentiation by isoflurane when the volume of the amino acid side chain increases.[62] They proposed that this residue may be an anesthetic binding cavity. The binding site of the general anesthetics for the GLIC is in the apo-structure in the upper part of the transmembrane domain of each protomer and accessible from membranes.[48] Xenon modulates the GLIC at or above clinical concentrations.[49] Ivermectin, which inhibits neurotransmission, binds with the glutamate-gated chloride channel (GluCl), and the binding site is within each subunit interface in the upper part of the transmembrane domain.[50] If there is a binding site for xenon molecules in the upper part of the transmembrane domain of proteins which relate to general anesthesia, the jamming of xenon molecules antagonizes the effects of xenon anesthetic according to the protein receptor hypothesis because xenon molecules cannot access to the binding site in the upper half of the membrane domain under high pressures. Moreover, since the properties of the membrane come close to those without xenon molecules under high pressures, the function of anesthetic will be decreased according to the membrane hypothesis. Therefore, on the basis of the membrane hypothesis or the protein receptor hypothesis, we have observed the pressure reversal by MD simulations for the first time. In the future, the mechanism of the pressure reversal will become more clear if the binding sites of general anesthetics will be found.

These results strongly suggest that xenon molecule acts as anesthetic when it moves freely in membranes. However, when the xenon molecule is pushed out between the upper and lower membrane, the function of anesthetic would be decreased. We suggest that the pressure reversal originates from a jamming of xenon molecules. This possible hypothesis is different from Pauling's hypothesis of hydrate-microcrystal theory of anesthesia.[63]

Xenon molecules are jammed in the center of membranes unlike a halothane molecule and an alcoholic molecule. Xenon molecules usually move to the direction perpendicular to the lipid molecules when they are in membranes, because membranes form comblike structures. In diffusions on comblike structures, molecules cannot move to a certain direction when molecules are in the teeth of the comb.[64] In membranes, comb structures are not static and the diffusion to the z direction is also subdiffusive. We think that subdiffusion of xenon molecules in membranes is related to the diffusion on comb structures and that anomalous transport of anesthetic in membranes would be an important subject.

ASSOCIATED CONTENT

Supporting Information

Figure S1 showing the density of the z position of xenon molecules at 350 K and Figure S2 showing change in the bilayer thickness and the gap between terminal carbons. This material is available free of charge via the Internet at http://pubs.acs.org.

AUTHOR INFORMATION

Corresponding Author

*E-mail: yasuoka@mech.keio.ac.jp. Phone: +81-45-566-1523. Fax: +81-45-566-1495.

Notes

The authors declare no competing financial interest.

■ ACKNOWLEDGMENTS

This work is supported by the Core Research for the Evolution Science and Technology (CREST) of the Japan Science and Technology Corporation (JST) and Keio University Program for the Advancement of Next Generation Research Projects.

■ REFERENCES

(1) Johnson, F. H.; Flagler, E. A. *Science* **1950**, *112*, 91.
(2) Halsey, M. J.; Wardley-Smith, B. *Nature* **1975**, *257*, 811.
(3) Lever, M. J.; Miller, K. W.; Paton, W. D. M.; Smith, E. B. *Nature* **1971**, *231*, 368.
(4) Miller, K. W.; Paton, W. D.; Smith, R. A.; Smith, E. B. *Mol. Pharmacol.* **1973**, *9*, 131.
(5) Simon, S. A.; Parmentier, J. L.; Bennett, P. B. *Comp. Biochem. Physiol.* **1983**, *75A*, 193.
(6) Chau, P. L. *Br. J. Pharmacol.* **2010**, *161*, 288.
(7) Meyer, H. *Naunyn-Schmiedebergs Arch. Pharmakol.* **1899**, *42*, 109.
(8) Overton, C. E.; Lipnick, R. L. *Studies of Narcosis*; Chapman and Hall: London, 1991.
(9) Heimburg, T.; Jackson, A. D. *Biophys. J.* **2007**, *92*, 3159.
(10) Trudell, J. R.; Hubbell, W. L.; Cohen, E. N. *Biochim. Biophys. Acta* **1973**, *291*, 321.
(11) Trudell, J. R.; Hubbell, W. L.; Cohen, E. N. *Biochim. Biophys. Acta* **1973**, *291*, 328.
(12) Tu, K.; Tarek, M.; Klein, M. L.; Scharf, D. *Biophys. J.* **1998**, *75*, 2123.
(13) Koubi, L.; Tarek, M.; Klein, M. L.; Scharf, D. *Biophys. J.* **2000**, *78*, 800.
(14) Koubi, L.; Saiz, L.; Tarek, M.; Scharf, D.; Klein, M. L. *J. Phys. Chem. B* **2003**, *107*, 14500.
(15) Stimson, L. M.; Vattulainen, I.; Róg, T.; Karttunen, M. *Cell. Mol. Biol. Lett.* **2005**, *10*, 563.
(16) Pickholz, M.; Saiz, L.; Klein, M. L. *Biophys. J.* **2005**, *88*, 1524.
(17) Griepernau, B.; Leis, S.; Schneider, M. F.; Sikor, M.; Steppich, D.; Böckmann, R. A. *Biochim. Biophys. Acta* **2007**, *1768*, 2899.
(18) Terama, E.; Ollila, O. H. S.; Salonen, E.; Rowat, A. C.; Trandum, C.; Westh, P.; Patra, M.; Karttunen, M.; Vattulainen, I. *J. Phys. Chem. B* **2008**, *112*, 4131.
(19) Griepernau, B.; Böckmann, R. A. *Biophys. J.* **2008**, *95*, 5766.
(20) Chau, P.-L.; Hoang, P. N. M.; Picaud, S.; Jedlovszky, P. *Chem. Phys. Lett.* **2007**, *438*, 294.
(21) Chau, P.-L.; Jedlovszky, P.; Hoang, P. N. M.; Picaud, S. *J. Mol. Liq.* **2009**, *147*, 128.
(22) Cantor, R. S. *Biochemistry* **1997**, *36*, 2339.
(23) Cantor, R. S. *J. Phys. Chem. B* **1997**, *101*, 1723.
(24) Jenkins, A.; Greenblatt, E. P.; Faulkner, H. J.; Bertaccini, E.; Light, A.; Lin, A.; Andreasen, A.; Viner, A.; Trudell, J. R.; Harrison, N. L. *J. Neurosci.* **2001**, *21*, RC136.
(25) Franks, N. P. *Nat. Rev. Neurosci.* **2008**, *9*, 370.
(26) Goto, T.; Suwa, K.; Uezono, S.; Ichinose, F.; Uchiyama, M.; Morita, S. *Br. J. Anaesth.* **1998**, *80*, 255.
(27) Petersen-Felix, S.; Luginbühl, M.; Schnider, T. W.; Curatolo, M.; Arendt-Nielsen, L.; Zbinden, A. M. *Br. J. Anaesth.* **1998**, *81*, 742.
(28) Froeba, G.; Marx, T.; Pazhur, J.; Baur, C.; Baeder, S.; Calzia, E.; Eichinger, H. M.; Radermacher, P.; Georgieff, M. *Anesthesiology* **1999**, *91*, 1047.
(29) Goto, T.; Nakata, Y.; Ishiguro, Y.; Niimi, Y.; Suwa, K.; Morita, S. *Anesthesiology* **2000**, *93*, 1188.
(30) Sanders, R. D.; Franks, N. P.; Maze, M. *Br. J. Anaesth.* **2003**, *91*, 709.
(31) Goto, T.; Hanne, P.; Ishiguro, Y.; Ichinose, F.; Niimi, Y.; Morita, S. *Anaesthesia* **2004**, *59*, 1178.
(32) Preckel, B.; Weber, N. C.; Sanders, R. D.; Maze, M.; Schlack, W. *Anesthesiology* **2006**, *105*, 187.
(33) Harris, P. D.; Barnes, R. *Anaesthesia* **2008**, *63*, 284.
(34) de Sousa, S. L. M.; Dickinson, R.; Lieb, W. R.; Franks, N. P. *Anesthesiology* **2000**, *92*, 1055.
(35) Franks, N. P.; Dickinson, R.; de Sousa, S. L. M.; Hall, A. C.; Lieb, W. R. *Nature* **1998**, *396*, 324.
(36) Yamakura, T.; Harris, R. A. *Anesthesiology* **2000**, *93*, 1095.
(37) Ogata, J.; Shiraishi, M.; Namba, T.; Smothers, C.; Woodward, J.; Harris, R. *J. Pharmacol. Exp. Ther.* **2006**, *318*, 434.
(38) Dickinson, R.; Peterson, B. K.; Banks, P.; Simillis, C.; Martin, J. C. S.; Valenzuela, C. A.; Maze, M.; Franks, N. P. *Anesthesiology* **2007**, *107*, 756.
(39) Liu, L. T.; Xu, Y.; Tang, P. *J. Phys. Chem. B* **2010**, *114*, 9010.
(40) Sobolevsky, A. I.; Rosconi, M. P.; Gouaux, E. *Nature* **2009**, *462*, 745.
(41) Nagele, P.; Metz, L. B.; Crowder, C. M. *Anesthesiology* **2005**, *103*, 508.
(42) Belelli, D.; Lambert, J. J.; Peters, J. A.; Wafford, K.; Whiting, P. *J. Proc. Natl. Acad. Sci. U. S. A.* **1997**, *94*, 11031.
(43) Mihic, S. J.; Ye, Q.; Wick, M. J.; Koltchine, V. V.; Krasowski, M. D.; Finn, S. E.; Mascia, M. P.; Valenzuela, C. F.; Hanson, K. K.; Greenblatt, E. P.; Harris, R. A.; Harrison, N. L. *Nature* **1997**, *389*, 385.
(44) Ueno, S.; Wick, M. J.; Ye, Q.; Harrison, N. L.; Harris, R. A. *Br. J. Pharmacol.* **1999**, *127*, 377.
(45) Krasowski, M. D.; Harrison, N. L. *Br. J. Pharmacol.* **2000**, *129*, 731.
(46) Jenkins, A.; Andreasen, A.; Trudell, J. R.; Harrison, N. L. *Neuropharmacology* **2002**, *43*, 669.
(47) Salmi, E.; Laitio, R. M.; Aalto, S.; Maksimow, A. T.; Långsjö, J. W.; Kaisti, K. K.; Aantaa, R.; Oikonen, V.; Metsähonkala, L.; Någren, K.; Korpi, E. R.; Scheinin, H. *Anesth. Analg. (Hagerstown, MD, U. S.)* **2008**, *106*, 129.
(48) Nury, H.; Van Renterghem, C.; Weng, Y.; Tran, A.; Baaden, M.; Dufresne, V.; Changeux, J.- P.; Sonner, J. M.; Delarue, M.; Corringer, P. J. *Nature* **2011**, *469*, 428.
(49) Weng, Y.; Yang, L.; Corringer, P. J.; Sonner, J. M. *Anesth. Analg. (Hagerstown, MD, U. S.)* **2010**, *110*, 59.
(50) Hibbs, R. E.; Gouaux, E. *Nature* **2011**, *474*, 54.
(51) Hirano, Y.; Okimoto, N.; Kadohira, I.; Suematsu, M.; Yasuoka, K.; Yasui, M. *Biophys. J.* **2010**, *98*, 1512.
(52) Akimoto, T.; Yamamoto, E.; Yasuoka, K.; Hirano, Y.; Yasui, M. *Phys. Rev. Lett.* **2011**, *107*, 178103.
(53) Hirschfelder, J. O.; Curtiss, C. F.; Bird, R. B. *Molecular Theory of Gases and Liquids*, Theoretical Chemistry Laboratory, University of Wisconsin; Wiley: New York, 1954; Vol. *26*.
(54) Case, D. A.; et al. *AMBER 10*; University of California: San Francisco, 2008.
(55) Leekumjorn, S.; Sum, A. K. *J. Phys. Chem. B* **2007**, *111*, 6026.
(56) Rappolt, M.; Hickel, A.; Bringezu, F.; Lohner, K. *Biophys. J.* **2003**, *84*, 3111.
(57) Gullingsrud, J.; Schulten, K. *Biophys. J.* **2004**, *86*, 3496.
(58) Gurtovenko, A. A.; Vattulainen, I. *J. Phys. Chem. B* **2008**, *112*, 1953.
(59) Tieleman, D. P.; Marrink, S. J.; Berendsen, H. J. C. *Biochim. Biophys. Acta* **1997**, *1331*, 235.
(60) Shaikh, S. R.; Brzustowicz, M. R.; Gustafson, N.; Stillwell, W.; Wassall, S. R. *Biochemistry* **2002**, *41*, 10593.
(61) Flenner, E.; Das, J.; Rheinstädter, M. C.; Kosztin, I. *Phys. Rev. E* **2009**, *79*, No. 011907.
(62) Koltchine, V. V.; Finn, S. E.; Jenkins, A.; Nikolaeva, N.; Lin, A.; Harrison, N. L. *Mol. Pharmacol.* **1999**, *56*, 1087.
(63) Pauling, L. *Science* **1961**, *134*, 15.
(64) Bouchaud, J.-P.; Georges, A. *Phys. Rep.* **1990**, *195*, 127.